Radio Science, Volume ???, Number , Pages 1?? ,

Interference Mitigation Using a Focal Plane Array

Chad K. Hansen[1], Karl F. Warnick[2], Brian D. Jeffs[3]

Department of Electrical and Computer Engineering
Brigham Young University
459 Clyde Building, Provo, UT 84602

J. Richard Fisher[4] and Richard Bradley[5]

National Radio Astronomy Observatory[6]
P. O. Box 2, Route 28/92
Green Bank, WV 2494

We consider the use of spatial filtering algorithms for radio frequency interference (RFI) mitigation in conjunction with a focal plane feed array of electrically small elements. Numerical simulations are used to study the performance of 7 and 19 element hexagonal dipole arrays with a 25 meter reflector at an operating frequency of 1612 MHz. Using the maximum-SNR algorithm to generate array weights, an interfering signal was attenuated by 40 dB or more. The effective sensitivity of the system, including interferer power in the system noise temperature, was comparable to the sensitivity attained in the absence of RFI. Moving the interferer through the reflector pattern sidelobes caused fluctuations in the gain and system sensitivity. This effect was exacerbated by a reflector model with random surface distortions. These results indicate that array feeds are a promising approach for RFI migitation, but achieving stable radiation patterns in the presence of an interferer may require a tradeoff between pattern control and maximum attainable sensitivity.

1. Introduction

Radio frequency interference (RFI) is a problem of growing significance in radio astronomy. When efforts by regulatory bodies to protect important bands from infringement by active sources and establish radio quiet zones fail to eliminate RFI, signal processing techniques must be used to mitigate received interference. Major classes of methods include time and frequency domain blanking [*Weber et al.*, 1999], adaptive cancellation and subtraction techniques [*Barnbaum and Bradley*, 1998; *Poulsen et al.*, 2003], and spatial filtering [*Smolders and Hampson*, 2002; *Raza et al.*, 2002; *Ellingson and Hampson*, 2002; *Ellingson*, 2003; *Jeffs et al.*, 2004]. A review of RFI mitigation methods and general considerations can be found in [*Fridman and Baan*, 2001]. In this paper, we investigate the use of an array feed in conjunction with a single large reflector to cancel an interfering signal using the spatial filtering approach.

Previous work on practical implementations and prototypes of RFI mitigation techniques includes real-time adaptive cancellation, time blanking, and spatial nulling systems at the National Radio Astronomy Observatory (NRAO) [*Fisher*, 1999, 2001]. RFI mitigation techniques are being implemented at the Australia Telescope National Facilty (ATNF) [*Briggs et al.*, 2000] and the Netherlands Foundation for Research in Astronomy (NFRA) [*Baan et al.*, 2002]. Simulations have also been widely used in studying RFI mitigation approaches. Russian geolocation satellite (GLONASS) signals have been cancelled using parametric signal modeling and subtraction [*Ellingson et al.*, 2001]. Auxiliary antenna assisted RFI mitigation approaches were investigated by *Jeffs et al.* [2004]. RFI mitigation is a key consideration in the design of future radio astronomy

[1]chad.hansen@ngc.com
[2]warnick@ee.byu.edu
[3]bjeffs@ee.byu.edu
[4]rfisher@nrao.edu
[5]rbradley@cv.nrao.edu
[6]The NRAO is operated for the National Science Foundation (NSF) by Associated Universities, Inc. (AUI) under a cooperative agreement.

0048-6604/05/$11.00

observatories, including the Allen Telescope Array (ATA) [*Bower*, 2002] and the Square Kilometer Array (SKA) [*Bell et al.*, 2000].

In order to implement spatial filtering methods, multiple correlated, spatially separated views of the interfering signal are required. This could be accomplished using an array of single-feed reflector antennas. But the effectiveness of spatial filtering is limited in this scenario, because the large separation between elements leads to grating lobes in the array pattern. The array response pattern can be controlled more completely with element spacings of less than one wavelength (although possibly at the expense of spatial resolution). This is realized by some of the proposed approaches for SKA antennas consisting of phased arrays of many elements [*Bij de Vaate and Kant*, 2002]. Another approach to implementation of spatial filtering techniques is to employ an array of electrically small feed antennas near the focal plane of a large reflector.

Array feeds are widely used in communications applications outside the field of radio astronomy, and the basic theory has been in continuous development for over thirty years [*Shelton*, 1965; *Rudge and Withers*, 1971; *Bird et al.*, 1978]. Phased array feeds allow correction of pattern distortion due to reflector surface aberrations [*Amitay and Zucker*, 1972] and electronic formation of multiple scanned beams [*Galindo-Isreal et al.*, 1978; *Mrstik and Smith*, 1981]. Array feeds are commonly used to obtain shaped gain patterns or achieve other pattern design criteria for such applications as satellite communications [*Reid and Bathker*, 1972; *Bird*, 1982; *Karimi and Blostein*, 1996; *Huang and Jamnejad*, 1989; *Singh and Kumar*, 1996; *Hall et al.*, 1989; *Perrott and Griffin*, 1991]. Phased array feeds have been used in radar applications for wide-angle scanning and improvement of the efficiency of off-axis beams of large-aperture reflectors [*Blank and Imbriale*, 1988].

Within the field of radio astronomy, most existing arrays have employed electrically large, waveguide type feeds, with each element individually matched to the reflector aperture for optimal sensitivity and minimal or no signal combining between elements [*Emerson and Payne*, 1995]. The benefits of this approach relative to arrays of electrically small elements are ease of implementation of the array, since standard elements can be used, and reduced signal processing requirements, as the signal paths for each element can be independent. Due to the large element spacing, this type of array can be viewed as an undersampled feed, as the fields across the focal plane of the reflector are not sampled finely enough to reconstruct the complete far field image across the field of view of the feed array and reflector system [*Fisher*, 1996]. An example of this type of feed is the multibeam "HIPASS" receiver on the Parkes telescope in Australia, which uses feed displacement to produce multiple beams without active array beamforming [*Stavely-Smith et al.*, 1996].

Fully sampled arrays of electrically small elements have received less attention in radio astronomy. Fully sampled feeds offer the ability to use holographic wavefront reconstruction techniques, compensate for reflector aberrations, improve the efficiency of off-axis beams, achieve shaped antenna patterns, and electronically synthesize multiple beams for rapid sky surveys with no coverage gaps across the field of view [*Blank and Imbriale*, 1988; *Fisher*, 1996; *Woo*, 1986]. The disadvantage is increased complexity of array signal processing, but with the current capability and low cost of DSP and FPGA solutions, a real-time system is feasible at present. NRAO has built and tested functional prototype array feeds, including an array of 19 sinuous elements [*Fisher and Bradley*, 1998; *Fisher et al.*, 1996; *Bradley et al.*, 1996; *Fisher and Bradley*, 2000]. Other contributions to the study of fully sampled array feeds include [*Ivashina and van't Klooster*, 2002]

In this paper, we are concerned with the application of array feeds to the problem of RFI mitigation. Before the array feed approach can be adopted as a solution for the RFI problem, its performance in the absence of an interferer must be comparable to that of a single feed. For this reason, we consider in some detail the no-interferer case. Using simulated radiation patterns, we determine the maximum attainable sensitivity with a seven element hexagonal array feed as a function of beam steering angle and offset of the feed away from the focal plane along the reflector axis. Values of the gain and spillover efficiency corresponding to optimal sensitivity are also given. These results are compared to beamformer weights optimized for maximum gain and to the conjugate field match (CFM) array weight solution. After quantifying the performance of the array feed in the absence of RFI, we introduce an interfering signal into the model, and determine the attainable effective sensitivity, where interferer power is considered to be part of the system noise. To explain observed behaviors of the beamformer in the presence of RFI,

we develop an analytical model for the optimal SNR, and compare the model to simulated results.

2. Array Feed Performance Without Interference

The primary performance metric for a focal plane array feed is high sensitivity for electronically formed beams. Other desirable qualities include large bandwidth and low gain fluctuation and beam shape distortion for steered beams. In order to establish a baseline for the system performance in the presence of an interfering signal, we consider these parameters for a seven element array feed in the no-interferer case.

We first review a few definitions in order to establish notation. As a figure of merit, we employ the system sensitivity

$$S_{sys}\ (\mathrm{Jy}^{-1}) = \frac{G\,(\mathrm{K/Jy})}{T_{sys}} \tag{1}$$

This quantity is proportional to signal to noise ratio at the receiver output, with equality for a source of unit intensity (1 Jy). Gain in units of K/Jy is related to the effective collecting area by

$$G\,(\mathrm{K/Jy}) = A_e \frac{10^{-26}}{2k_B} \tag{2}$$

where $k_B = 1.38\times10^{-23}$ J/K is Boltzman's constant. The factor of two in the denominator is included because the signal power is assumed to be divided equally between two polarizations (a gain of 1 K/Jy corresponds to an effective aperture of 2760 m^2).

The system temperature T_{sys} is the sum of receiver, spillover, atmospheric, and cosmic background temperatures,

$$T_{sys} = T_{rec} + T_{spill} + T_{atmosphere} + T_{cmb}. \tag{3}$$

where

$$T_{spill} = (1-\eta_{spill})T_{ground}\ . \tag{4}$$

While antennas for astronomy are operated as receivers, spillover efficiency is most easily defined as the efficiency of illumination of the reflector surface by transmitted power from the feed, so that

$$\eta_{spill} = \frac{P_{refl}}{P_{tot}} \tag{5}$$

where, taking the transmitting case, P_{refl} is the power illuminating the reflector and P_{tot} is the total power radiated by the array. We assume that the array elements have a hemispherical radiation pattern and that the antenna is pointed to zenith. For all of the simulations in this paper, $T_{rec} = 15\,\mathrm{K}$, $T_{atmosphere} = T_{cmb} = 0$, and $T_{ground} = 250\,\mathrm{K}$. We neglect noise due to atmospheric and cosmic background radiation. The same noise model would result from reducing T_{rec} slightly and setting $T_{atmosphere}$ and T_{cmb} to appropriate nominal values, while ignoring the small correlation of atmospheric noise and cosmic background radiation at the array.

For convenience, in computing gain, aperture and spillover efficiencies, and system sensitivity, we treat the antenna as if it were a transmitter rather than a receiver. Reciprocity allows received signals to be expressed in terms of radiated fields. Let the electric field radiated by the nth array element in isolation from the reflector and other array elements be denoted by $\overline{E}_n^{inc}$. The pattern overlap matrix is

$$A_{mn} = \frac{1}{2\eta P_m}\int \overline{E}_m^{inc*}\cdot\overline{E}_n^{inc}\, r^2 d\Omega \tag{6}$$

where η is the characteristic impedance of free space and P_n is the total power radiated by the nth element in isolation. The normalization is such that the diagonal elements of A are unity. If the feed elements are identical and mutual coupling is neglected, then the P_m are all equal, so that $P_m = P_1$. Received signals at each array element are combined using the complex weights $\mathbf{w} = [w_1\ w_2\ \ldots\ w_N]^T$.

The pattern overlap matrix for spillover is defined as

$$A_{spill,mn} = \frac{1}{2\eta P_m}\int_{spill} \overline{E}_m^{inc*}\cdot\overline{E}_n^{inc}\, r^2 d\Omega \tag{7}$$

where the elevation angle of the integration extends from the reflector rim to a plane perpendicular to the axis of the reflector. The spillover efficiency can be expressed as

$$\eta_{spill} = 1 - \frac{\mathbf{w}^{\mathrm{H}}\mathbf{A}_{spill}\mathbf{w}}{\mathbf{w}^{\mathrm{H}}\mathbf{A}\mathbf{w}} \tag{8}$$

and is equal to unity for an ideal illumination pattern without spillover.

In order to compute the system sensitivity S_{sys} in (1), we must define the gain or effective aperture of the array and reflector system. The appropriate measure of directivity for a receiving array is the array gain

$$G_a = \frac{\mathrm{SNR}_{out}}{\mathrm{SNR}_{in}} \tag{9}$$

To obtain a meaningful aperture efficiency, we need to determine the signal gain of the array without including the effects of noise reduction due to the

beamformer and net signal power amplification due to a common gain factor in the beamformer weights $\mathbf{w}$. For this reason, we take the input SNR to be the ratio of the signal power received by an isotropic antenna in one polarization to the noise power received by an antenna with the same spillover efficiency as the receive array, so that

$$\mathrm{SNR}_{in} = \frac{\lambda^2 S^{sig}}{8\pi k_B (1-\eta_{spill}) T_{ground}} \tag{10}$$

where S^{sig} is the power flux density of the signal. In this case, it can be shown that $G_a = G$, where G is the gain of a transmitting array with the same beamformer weights as the receiving array. Other choices for the noise model and input SNR in the definition of array gain are common in the signal processing literature, but for our purposes (10) is preferable because other models can lead to effective apertures larger than the physical area of the reflector.

With this choice of input SNR, the array gain of the feed and reflector system becomes

$$G = \frac{2\pi}{\eta P_1} \frac{|\mathbf{w}^{\mathrm{H}} \mathbf{E}^s|^2}{\mathbf{w}^{\mathrm{H}} \mathbf{A} \mathbf{w}} \tag{11}$$

where $\mathbf{E}^s = \left[\hat{p}\cdot\overline{E}_1\ \hat{p}\cdot\overline{E}_2\ \ldots\ \hat{p}\cdot\overline{E}_N\right]^T$ and $\overline{E}_n$ is the field radiated by the nth array element in the presence of the reflector when excited as a transmitter. $\hat{p}$ is a unit vector in the direction of the received polarization. The aperture efficiency is

$$\eta_{ap} = \frac{\lambda^2 G}{4\pi A} \tag{12}$$

where A is the physical area of the reflector aperture.

The signal correlation matrix at the element feed ports is

$$\mathbf{R}_{ss} \equiv E[\mathbf{x}_s^{\mathrm{H}} \mathbf{x}_s] = \frac{\lambda^2 S^{sig}}{4\eta P_1 k_B} \mathbf{E}^{s*} \mathbf{E}^{sT} \tag{13}$$

where $\mathbf{x}_s$ is a vector containing time samples of the signal at the array elements. The spillover and receiver noise correlation matrix is

$$\mathbf{R}_{nn} = T_{rec}\mathbf{I} + T_{ground}\mathbf{A}_{spill} \tag{14}$$

where we have ignored correlation of LNA noise due to mutual coupling between the array elements. With these definitions, the system sensivitity (1) can be expressed as

$$S_{sys} = \frac{\mathbf{w}^{\mathrm{H}} \mathbf{R}_{ss} \mathbf{w}}{\mathbf{w}^{\mathrm{H}} \mathbf{R}_{nn} \mathbf{w}} \tag{15}$$

with the signal flux density $S^{sig} = 1\,\mathrm{Jy}$.

2.1. Gain and Sensitivity Optimization

The simplest beamformer is the conjugate field match solution,

$$\mathbf{w}_{CFM} = \mathbf{E}^{s*} \tag{16}$$

The quadratic forms in Eqs. (11) and (15) can be maximized using standard techniques. The array weights for maximum gain are given by

$$\mathbf{w}_{G,max} = \mathbf{A}^{-1}\mathbf{E}^{s*} \tag{17}$$

For a linear array feed, it has been shown that CFM closely approximates the maximum gain of a linear array if the element spacing is greater than 0.5λ [*Lam et al.*, 1985]. The array weights for maximum system sensivity (SNR) are

$$\mathbf{w}_{S,max} = \mathbf{R}_{nn}^{-1}\mathbf{E}^{s*} \tag{18}$$

where we have used the fact that $\mathbf{R}_{ss}$ in (15) is a rank one matrix.

While the focus of the present study is on narrowband signals, bandwidth is of great importance in science applications. It has long been known that for closely spaced arrays, optimal gain solutions may enter a superdirectivity regime, characterized by unacceptably large sensitivity of directivity to small fluctuations in array element weights and low bandwidth. To ensure that such is not the case for the optimal solutions considered here, we compute the geometrical Q factor

$$Q_g = \frac{\mathbf{w}^{\mathrm{H}}\mathbf{w}}{\mathbf{w}^{\mathrm{H}} A \mathbf{w}} \tag{19}$$

The Q of the array system at the output port of the beamformer is given approximately by the geometrical quality factor Q_g multiplied by the Q of a single isolated element [*Uzsoky and Solymar*, 1956], which is typically on the order of unity.

2.2. Reflector and Feed Parameters

Array elements are located on a hexagonal grid with a spacing of 0.6 wavelengths between elements. The dipoles are y-directed and located such that one of the elements lies at $x = 0.6\,\lambda$ relative to the center element. The operating frequency is 1612 MHz ($\lambda = 18.6\,\mathrm{cm}$). This spacing is small enough to fully sample the focal plane fields [*Fisher and Bradley*, 1999], and large enough that mutual coupling is not an overwhelming problem. A ground plane was not used for ease of simulation, but the radiation pat-

terns of the array elements were assumed to be hemispherical in computing received spillover noise and efficiency. The ground plane should be included in future work, especially when considering broadband arrays and the effects of mutual coupling. Support struts are also not included in the model.

Candidates for feed elements include sleeved or folded dipoles [*Hsiao and Wong*, 2004] and Vivaldi antennas [*Shin and Schaubert*, 1999], where the selection is governed primarily by bandwidth and physical size. Noise performance is another important consideration. In order to simplify the present study, we take the elements to be Hertzian dipoles. As the radiation pattern of a Hertzian dipole is similar to that of other small antennas, results should be close to that obtained with more realistic elements.

The reflector is a 25 m paraboloid with $f/D = 0.36$. Two surface models are considered, one with no distortion, and another including random distortion of $\lambda/16$ (1.16 cm) peak-to-peak amplitude. The correlation length of the distortion is 50 cm.

2.3. Numerical Results

In order to compute radiated fields for the array and reflector system, we use the GRASP8-SE (TICRA, www.ticra.com) physical theory of diffraction antenna simulation software package. The radiated fields are used to obtain the receive array element responses to a point signal source located in the boresight direction according to Eq. (13), and the thermal noise correlation matrix is computed from (14).

Figure 1 shows the maximum sensitivity of the seven-element array feed as a function of offset distance along the paraboloid axis relative to the focal plane. Figure 2 shows the gain and spillover efficiency of the array. The highest sensitivity is achieved at the focal plane. We note that only a small offset is required before the array is smaller than the geometrical optics cone of the fields focused by the reflector and cannot capture all energy available from the reflector.

For the optimal sensitivity beamformer, the aperture efficiency at zero axial feed offset neglecting blockage and feed support scattering was 47% and the spillover efficiency was 99.2%. For the optimal gain beamformer, the aperture efficiency was 70.4% and the spillover efficiency was 80.9%. As a reference point for these results, the measured aperture efficiency for a single hybrid mode scalar feed is roughly 50%. Using measured radiation patterns to compute efficiency without blockage, efficiency increases to perhaps 65%. Due to observed discrepancies between measured gain and gain computed from feed radiation patterns, the simulated values in this paper ought to be compared to the latter figure for the scalar feed, rather than the former. For these results, to speed up the simulations the radiation patterns were computed using the PO-based line integral method of *Imbriale et al.* [1974], which is very close to GRASP8 near the main lobe.

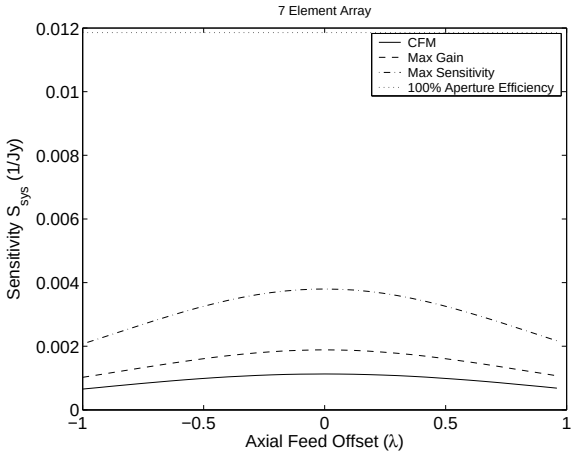

Figure 1. Sensitivity as a function of feed displacement away from the focal plane for a seven element dipole hex array, with respect to various choices of the array beamformer weights. The feed remains symmetrically placed with respect to the reflector axis and is displaced away from or towards the reflector.

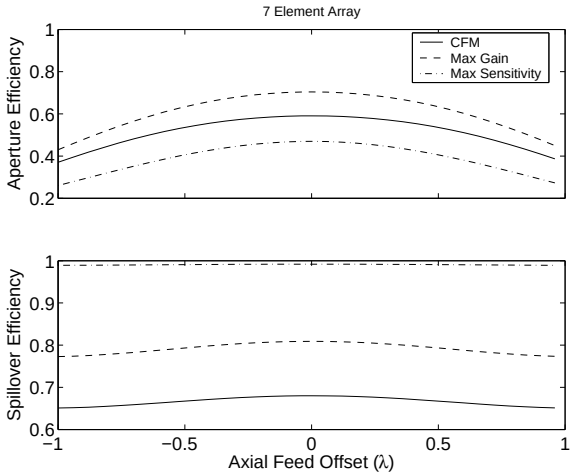

Figure 2. Aperture and spillover efficiencies for the same sets of array weights as in Fig. 1.

In a traditional single-feed system, it is possible to perform beam steering by displacing the feed in a lateral direction. By optimizing the array weights for maximum sensitivity in an off-boresight direction, beam steering can also be achieved with an array feed. The array is not moved. A key question is how far a single beam can be steered while still maintaining high sensitivity with a phased array feed. Sensitivity as a function of angle for a steered beam can be seen in Figure 3, for arrays at several offset distances relative to the focal plane. If the array were larger, the beam could be steered further without sensitivity loss. The sensitivity in Figure 3 increases as the steering angle changes from 0° to 1°. For the boresight beam the majority of the power is received by the center element, whereas for a source at 0.3° away from boresight, the field distribution in the plane of the array feed is large near two elements of the array, which likely accounts for the increased gain and sensitivity for the steered beam. If mutual coupling between array elements were included in the model, the sensitivity increase may be less pronounced.

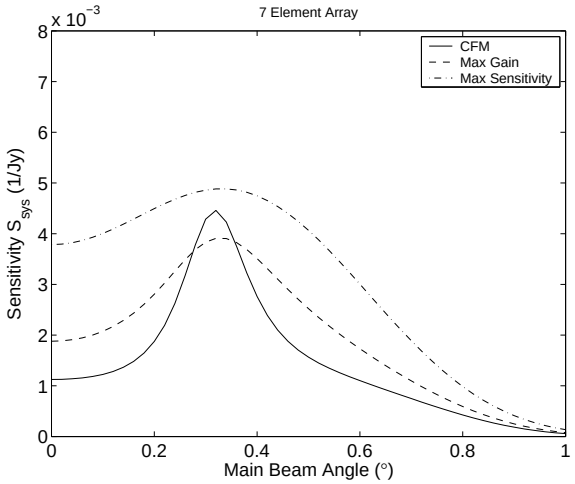

Figure 3. Sensitivity as a function of steered beam angle.

In order to ensure that the optimal gain and sensitivity solutions are not in the superdirectivity regime, we also compute the geometrical Q-factor in Eq. (19). Results are shown in Fig. 4, which shows Q_g versus array element spacing. These results indicate that at $0.6\,\lambda$, the Q-factor is acceptably low. For a broadband system, high gain and sensitivity beamformer solutions at the low end of the band, for which element spacing is small relative to the wavelength, would require an additional constraint on Q_g in order to avoid the superdirectivity regime.

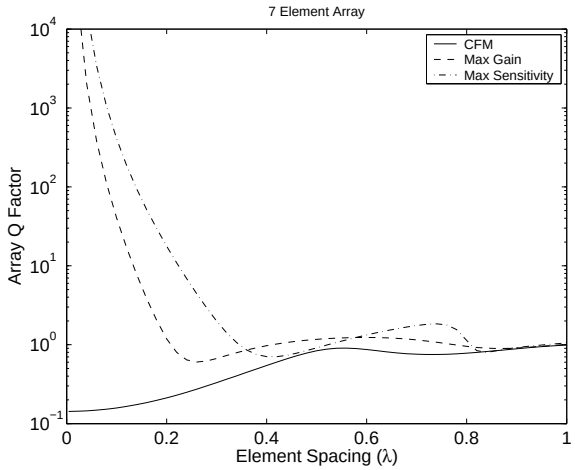

Figure 4. Geometrical Q-factor as a function of element spacing for the seven element array. The operating frequency is swept and the physical element locations are fixed. At $0.6\,\lambda$, the Q-factor is acceptably small, but increases rapidly for a fixed physical array size as the operating frequency decreases.

3. RFI Mitigation

Having established the performance of the array feed in the no-interferer case, we now turn to the primary goal of this study, the cancellation of an interfering signal using a spatial filtering algorithm. We seek to determine if interference mitigation can be achieved while still maintaining high gain and spillover efficiency. Particular attention will be paid to gain fluctuations as the interferer moves through the antenna sidelobes.

Weak astronomical signals are typically detected as a small perturbation of a temporally or spectrally averaged thermal noise power baseline. The limiting factor in determining the weakest signal that can be observed is the standard deviation of the integrated thermal noise. Without interference, the relationship between instantaneous SNR and the ratio of signal power to noise standard deviation after integration is a simple proportionality. Because interfering signals are likely to be temporally nonstationary and spectrally nonwhite, they have a more severe impact on observations than thermal noise. The appropriate system performance metric is the ratio of signal power to the sum of the interference power and the thermal noise standard deviation. For very short integration times, this reduces to the instantaneous signal to interference and noise ratio (SINR) or alternatively, the effective sensitivity

$$S_{\mathit{eff}} = \frac{G}{T_{sys} + T_{int}} \tag{20}$$

which is analogous to the sensitivity S_{sys} as defined in Eq. (1) but includes interference power in the system noise temperature. A more specific measure of effective sensitivity might include a weighting factor that accounts for the effects of integration in reducing the thermal noise variance.

The most obvious choice for a beamformer is the max-SNR algorithm [*Mailloux*, 1994]. This beamformer is important because it provides an upper bound on sensitivity relative to any other set of of array weights. Practical considerations such as the lack of exactly known signal and interferer correlation matrices and the need for high gain stability will likely require that more sophisticated algorithms be used in a real system. We will refer to the beamformer as max-SINR when effective sensitivity S_{eff} is maximized, in order to distinguish this beamformer from the maximum sensitivity solution (18) in the no-interferer case.

The max-SINR weights are given by

$$\mathbf{w} = \underset{\mathbf{w}}{\operatorname{argmax}} \frac{\mathbf{w}^H \mathbf{R}_{ss} \mathbf{w}}{\mathbf{w}^H \mathbf{R}_{NN} \mathbf{w}} \tag{21}$$

where the thermal noise and interferer correlation matrix is

$$\mathbf{R}_{NN} = \mathbf{R}_{nn} + \mathbf{R}_{ii} \tag{22}$$

and $\mathbf{R}_{nn}$ is given by Eq. (14). For a single plane wave interferer signal, $\mathbf{R}_{ii}$ has the form of (13) but with the fields evaluated in the direction of the interferer arrival. For multiple uncorrelated interferers, $\mathbf{R}_{ii}$ can be taken to be the sum of single plane wave correlations.

The optimal weights are given by the solution to the generalized eigenvalue problem

$$\mathbf{R}_{ss}\mathbf{w} = \lambda_{\max}\mathbf{R}_{NN}\mathbf{w} \tag{23}$$

where $\lambda_{\max}$ is the largest eigenvalue. For a narrowband signal, exactly known signal and noise correlation matrices, and a single interferer, the max-SINR beamformer can be shown to yield the same solution as another common beamformer, the linearly constrained minimum variance (LCMV) algorithm. Because the signal is taken to be a plane wave, the max-SINR weights reduce to

$$\mathbf{w}_{S_{\mathit{eff},max}} = {\mathbf{R}_{NN}}^{-1}\mathbf{E}^{s*} \tag{24}$$

For large interference power levels and a point interference source, $\mathbf{R}_{NN}$ is nearly singular, in which case solving the generalized eigenvalue problem is more stable numerically.

In order to understand the performance of the array feed in the presence of RFI from a theoretical point of view, we consider the SINR attained by the max-SINR algorithm. If the signal correlation matrix is expressed in the form

$$\mathbf{R}_{ss} = \sigma_s^2 \mathbf{d}_s \mathbf{d}_s^{\mathrm{H}} \tag{25}$$

where $\mathbf{d_s}$ is the normalized array response vector $\mathbf{E}^{s*}/\|\mathbf{E}^s\|$, then it can be shown that the optimal SINR is

$$\mathrm{SINR} = \sigma_s^2 \mathbf{d}_s^H \mathbf{w} \tag{26}$$

where $\mathbf{w} = {\mathbf{R}_{NN}}^{-1}\mathbf{d}^s$. Using the matrix inversion lemma $\mathbf{R}_{NN}^{-1}$ can be found as

$$\mathbf{R}_{NN}^{-1} = \left(\mathbf{R}_{nn} + \sigma_i^2 \mathbf{d}_i \mathbf{d}_i^H\right)^{-1} \tag{27}$$

$$= \mathbf{R}_{nn}^{-1} - \frac{\sigma_i^2 \left(\mathbf{R}_{nn}^{-1}\mathbf{d}_i\right)\left(\mathbf{d}_i^H \mathbf{R}_{nn}^{-1}\right)}{1 + \sigma_i^2 \mathbf{d}_i^H \mathbf{R}_{nn}^{-1}\mathbf{d}_i} \tag{28}$$

where for convenience we have also defined the normalized interferer response to be $\mathbf{d}_i = \mathbf{E}^{i*}/\|\mathbf{E}^i\|$. We then have

$$\mathbf{w} = \mathbf{R}_{nn}^{-1}\mathbf{d}_s - \frac{\sigma_i^2 \mathbf{R}_{nn}^{-1}\mathbf{d}_i \mathbf{d}_i^H \mathbf{R}_{nn}^{-1}\mathbf{d}_s}{1 + \sigma_i^2 \mathbf{d}_i^H \mathbf{R}_{nn}^{-1}\mathbf{d}_i} \tag{29}$$

From Eq. (26),

$$\mathrm{SINR} = \sigma_s^2 \mathbf{d}_s^H \left[\mathbf{R}_{nn}^{-1}\mathbf{d}_s - \frac{\sigma_i^2 \mathbf{R}_{nn}^{-1}\mathbf{d}_i \mathbf{d}_i^H \mathbf{R}_{nn}^{-1}\mathbf{d}_s}{1 + \sigma_i^2 \mathbf{d}_i^H \mathbf{R}_{nn}^{-1}\mathbf{d}_i}\right] \tag{30}$$

From this expression, it can be seen that SNR is composed of two parts. The first component is the SNR obtained in the no-interferer case,

$$\mathrm{SNR}_0 = \sigma_s^2 \mathbf{d}_s^H \mathbf{R}_{nn}^{-1}\mathbf{d}_s \ . \tag{31}$$

and the second component is the degradation of SNR due to the interferer.

If we neglect the off-diagonal terms of $\mathbf{R}_{nn}$ due to the correlation of spillover noise arriving at different array elements, then the second term in (30) relative to SNR_0 becomes

$$\frac{\mathrm{INR}}{1 + \mathrm{INR}} |\mathbf{d}_i^H \mathbf{d}_s|^2 \tag{32}$$

where INR is the interferer to noise ratio σ_i^2/σ_n^2. The vector inner product can be identified as the squared cosine of the angle ψ between the response vectors $\mathbf{d}_s$ and $\mathbf{d}_i$. The optimal SINR in this case can be expressed as

$$\mathrm{SINR} = \mathrm{SNR}_0 \left(1 - \frac{\mathrm{INR}}{1 + \mathrm{INR}} \cos^2 \psi\right) \tag{33}$$

From this expression, it is apparent that when the array response to the interferer is similar to the signal response, the maximum achievable sensitivity drops. In the limit of large interferer intensity, this expression becomes

$$\mathrm{SINR} = \mathrm{SNR}_0 \left(1 - \cos^2 \psi\right) \tag{34}$$

If the correlation of spillover noise cannot be neglected, then the angle cosine in (34) is modified to the weighted angle cosine

$$\cos^2 \hat{\psi} = \frac{|\mathbf{d}_i^H \mathbf{R}_{nn}^{-1}\mathbf{d}_s|^2}{\mathbf{d}_s^{\mathrm{H}} \mathbf{R}_{nn}^{-1}\mathbf{d}_s \mathbf{d}_i^{\mathrm{H}} \mathbf{R}_{nn}^{-1}\mathbf{d}_i} \tag{35}$$

$\hat{\psi}$ can be interpreted as the angle between the signal and interferer response vectors in the norm induced by the inverse of the thermal noise correlation matrix.

An alternative physical interpretation for this result can be obtained by observing that the vector $\mathbf{w}_\circ = \mathbf{R}_{nn}^{-1}\mathbf{d}_s$ is the optimizer of the quadratic form

$$\frac{|\mathbf{w}^T \mathbf{d}_s^*|^2}{\mathbf{w}^{\mathrm{H}} \mathbf{R}_{nn} \mathbf{w}^{\mathrm{H}}} \tag{36}$$

which is equivalent to Eq. (15) for the SNR in the no-interferer case. The numerator of (35) is the squared interferer power received by the beamformer with weights $\mathbf{w}_\circ$. Thus, the SINR degradation term in (30) is governed by the interferer power received by the max-SNR beamformer (which uses no information about the interferer). If the max-SNR beamformer receives a large amount of interferer power, then the max-SINR beamformer performance degrades.

3.1. Numerical Results

As in the no-interferer case of the previous section, thermal radiation is assumed to arrive at the feed from a warm 250 K background over the solid angle extending in elevation angle from the reflector rim to the horizontal plane, assuming that the reflector axis is vertical. The interferer is a point source at some angle relative to the reflector axis (boresight), and the interferer power level is referenced using the received interferer power at the feed port of the center feed element relative to the thermal noise at the center element. The azimuth angle of the interferer is 0°. Similar results are obtained for other azimuth angles.

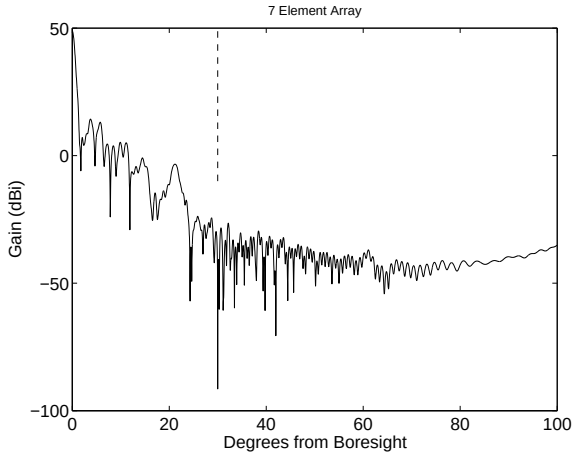

Figure 5. Beam pattern using max-SINR to cancel an interferering signal with arrival angle 30° away from boresight. The INR is 10 dB at the center element feed port.

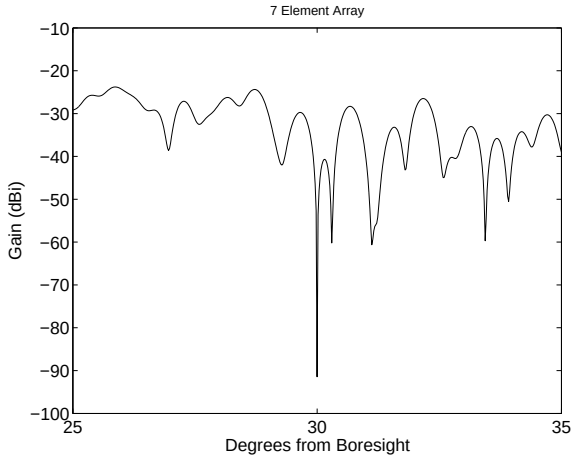

Figure 6. Detail of gain pattern null in the direction of the interferer.

Figure 5 shows the beam pattern for an interferer arrival angle of 30° and interference-to-noise ratio (INR) of 10 dB at the center feed element. The ratio of the interferer flux density to the signal flux density is 113 dB. Figure 6 shows a detail of the null placed in the direction of the interferer. Use of spatial filtering to suppress RFI leads to main beam shape distortion, as shown in Fig. 7. The angle of maximum gain is shifted slightly away from boresight. The beamformer is stable stable in the limits of large and small interferer powers (Fig. 8).

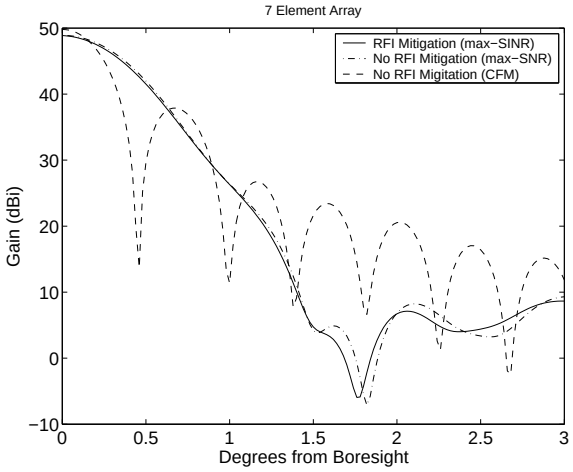

Figure 7. Gain pattern of the array feed using max-SNR and max-SINR. For comparison, the CFM solution is also shown. In the presence of interference, the max-SINR beamformer leads to small perturbations of the main beam relative to the no-interference case.

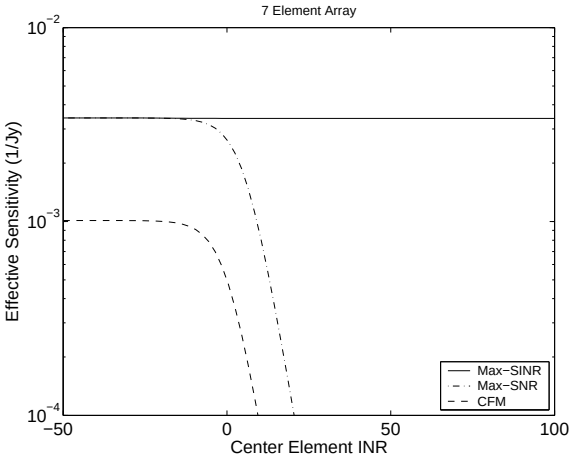

Figure 8. Effective sensitivity vs. INR at the center feed element for the phased array. The interferer arrival angle is 30° from boresight. The solid curve is the max-SINR solution, and the other curves are beamformers that do not suppress the interfering signal.

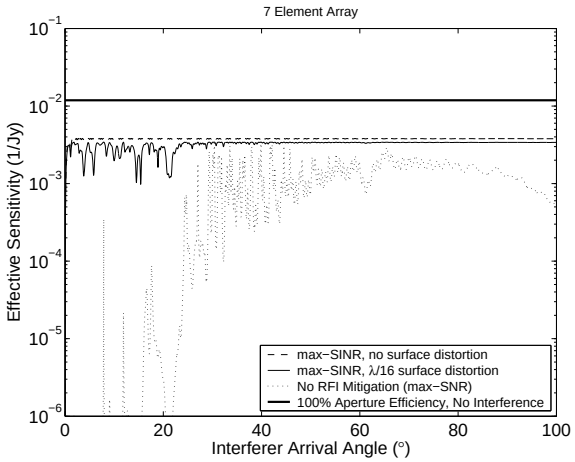

Figure 9. Effective sensitivity as a function of interferer location using max-SINR. Reflector surface distortion of 1.16 cm ($\lambda/16$) peak-to-peak amplitude leads to fluctuation in the maximum attainable effective sensitivity with respect to interferer arrival angle. Using a beamformer that does not suppress RFI (max-SNR) results in a substantial degradation of effective sensitivity.

Figure 9 shows the effective sensitivity as a function of interferer arrival angle. The corresponding aperture and spillover efficiencies are shown in Fig. 10. The flux density of the interferer is the same as that in Fig. 5. For a smooth reflector surface, the beamformer performance is stable with respect to interferer position. The effective sensitivity is much better than that obtained without RFI mitigation, and the margin of improvement increases as the interferer intensity becomes larger. Figure 11 shows the performance for two interfering sources, one moving and the other fixed at horizontal, representing a ground-based interferer. The intensity of the ground-based source is 20 dB greater than the moving interferer.

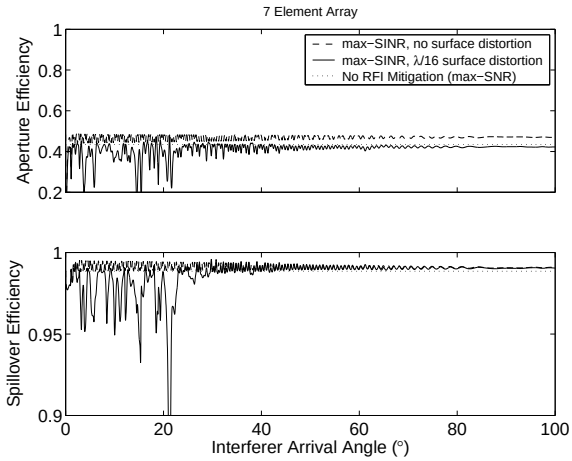

Figure 10. Aperture and spillover efficiencies as a function of interferer location using max-SINR, corresponding to the single-interferer case of Fig. 9.

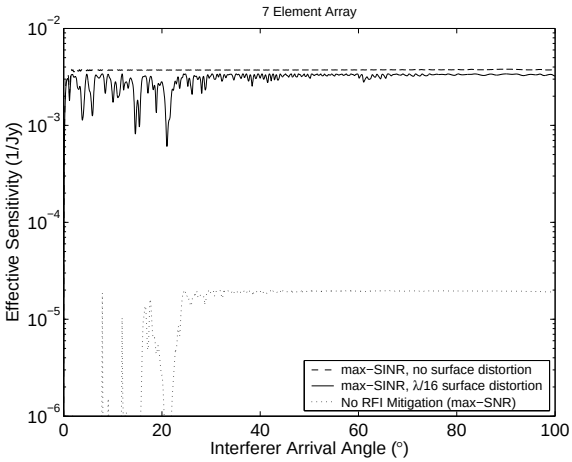

Figure 11. Similar to Fig. 9 but with two interferers, one moving and the other fixed at 90° from boresight with 20 dB greater intensity than the moving interferer, simulating a ground-based radio source.

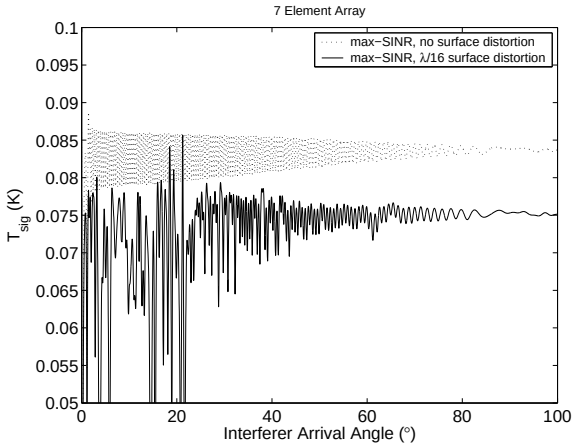

Figure 12. Signal output power as a function of interferer location using max-SINR beamformer. T_{sig} is shown on a linear scale so small fluctuations in system gain ("pattern rumble") are evident.

It can be seen in Fig. 9 that reflector surface distortion causes dramatic fluctuations in the effective sensitivity fluctuates as the interferer moves. Variations occur for smaller peak-to-peak surface distortion amplitudes if the correlation length of the distortion is also small. This has at least two adverse consequences for astronomical observations. First, sensitivity loss obviously limits the observation capability of the instrument to stronger sources. Second, fluctuations in received signal power as the interferer moves could be catastrophic to accurate measurements requiring high temporal gain stability. Fig. 12 shows the signal power at the beamformer output as the interferer moves in angle on a linear scale in order to show more clearly the degree of "pattern rumble" as the interferer moves. The system gain also fluctuates for the smooth reflector surface, but with smaller amplitude.

The decrease in effective sensitivity at some arrival angles is not due to inability to reject the interferer. The conventional sensitivity as defined in Eq. (1) is only negligibly different from effective sensitivity, meaning that very little interferer power is received. Figure 13 shows a plot of the interference rejection ratio (IRR) achieved with max-SINR. The IRR is the ratio of the interferer power at the beamformer output to the interferer power at the output without RFI mitigation, using the max-SNR algorithm to maximize the signal to thermal noise ratio. The IRR is at least 40 dB for all interferer arrival angles. While the interferer signal is rejected for all arrival angles, system sensitivity fluctuates because the gain and spillover efficiency achieved by the beamformer change as it adapts to the interferer array response.

Because max-SINR yields optimal sensitivity, sensitivity fluctuations cannot be overcome by making use of a different array processing algorithm. Instead, the number or placement of array elements must be modified. Displacing the seven element array away from the focal plane up to one wavelength in the boresight direction did not overcome the decrease in sensitivity. Changing the spacing between array elements by scaling as well as random perturbations also did not improve performance significantly. These results imply that the only way to achieve a more uniform sensitivity characteristic, barring some radical change in the basic approach, is to design a beamformer with a constant, suboptimal sensitivity constraint, and that increasing the overall sensitivity requires more array elements. The latter possibility is considered in the next section.

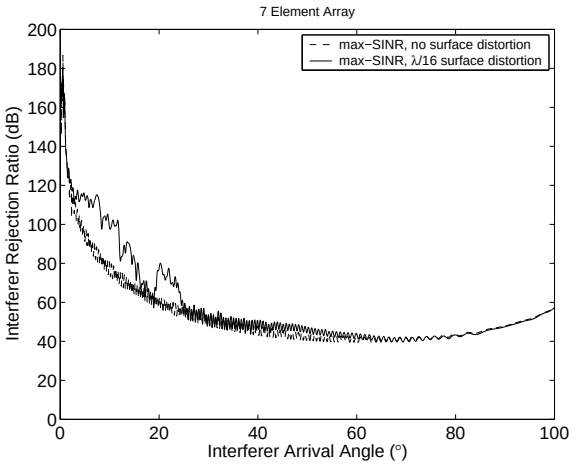

Figure 13. Interference rejection ratio (IRR) as a function of interferer location using max-SINR. The IRR is the ratio of the interferer power at the beamformer output to the interferer power at the output without RFI mitigation using the max-SNR beamformer.

3.2. 19-element Array

In this section, we study the increase in performance obtained with a larger feed array. For a 19 element hexagonal array, Fig. 14 shows the resulting effective sensitivity S_{sys} for the same noise and interferer models used in the previous section.

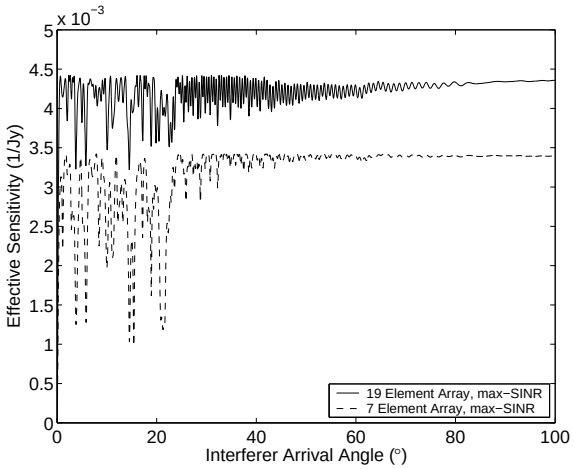

Figure 14. Effective sensitivity vs. interferer arrival angle for the 7 and 19 element phased array feeds using max-SINR. The reflector model includes a $\lambda/16$ peak-to-peak random surface distortion.

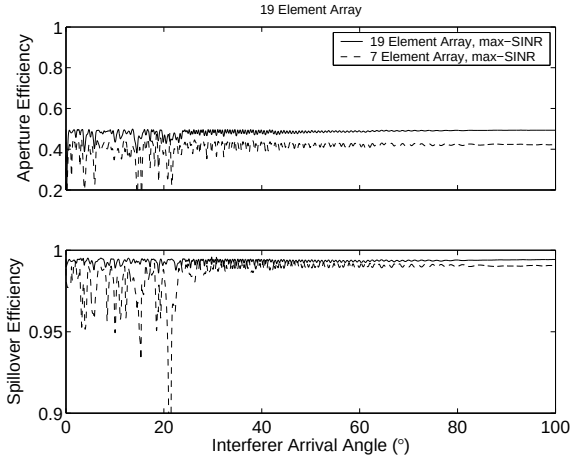

Figure 15. Aperture and spillover efficiency vs. interferer arrival angle for the 7 and 19 element phased array feeds using max-SINR.

As expected, the 19-element array produced a higher effective sensitivity than the 7-element array. The variability of the sensitivity for the 19 element array is slightly less in a relative sense than that of the smaller array, but fluctuations still occur. These results are for a reflector model with surface distortion. Gain fluctuations are smaller for a smooth reflector surface. As with the 7 element array, the 19 element array was displaced in the boresight direction away from the focal plane, but the focal plane array achieved the highest effective sensitivity.

Figure 15 shows the aperture and spillover efficiency of the 19-element array as a function of interferer arrival angle. These results show that both gain and spillover efficiency loss are responsible for the variations in effective sensitivity. In Fig. 16, the effective sensitivity for the 19 element array with a moving interferer is shown together with the approximation (33), which neglects the influence of thermal noise correlation on the max-SINR beamformer. It can be inferred from Eq. (33) that similarity between the interferer and signal response vectors after scattering from the reflector surface causes some of the SINR degradation. Correlated spillover noise exacerbates the effect. The SNR fluctuations might be viewed as a grating-lobe-like phenomenon, since the beamformer is unable to distinguish the signal and interferer due to the similarity of the array responses.

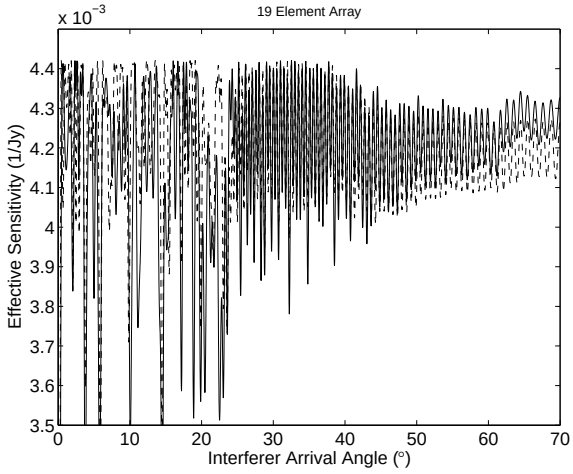

Figure 16. Effective sensitivity (SINR for 1 Jy intensity signal) for a moving interferer. The dashed line is the approximation (33), which neglects the influence of thermal noise correlation on the max-SINR beamformer.

4. Conclusions

We have shown using numerical simulations that a seven-element hexagonal dipole array feed, in the absence of an interfering signal, can attain aperture and spillover efficiencies that are comparable to a standard scalar feed. These results corroborate previous studies which indicate that array feeds are a promising approach for radio astronomy applications. We

have also investigated the effect of defocusing the feed by displacing it relative to the focal plane along the reflector axis, and found that the focal plane array provided the greatest sensitivity for the parameter values used in the simulations. For a 25 meter reflector operating at 19 cm wavelength, beams could be steered electronically, without moving the array, to 0.5° from boresight before sensitivity falls below the boresight value. If the array were larger, beams could be steered further before significant sensitivity loss occured.

We have also demonstrated that RFI mitigation is possible using an array of electrically small elements. Using a classical spatial filtering algorithm to generate array weights, an interfering signal was attenuated by 40 dB or more. For some interferer locations, the effective sensivitity, or the ratio of signal to system noise and interferer power, was comparable to the sensitivity in the no-interferer case. But for a reflector surface with random distortion and a moving interferer, the maximum attainable sensitivity fluctuated as a function of arrival angle of the interfering signal. This behavior was shown to be caused in part by similarity between the signal and interferer array responses. The fluctuations in sensitivity were not ameliorated by changing element spacing or displacing the feed away from the focal plane. Because of the optimality of the beamformer, these results represent the best performance over all possible array weights, so that improving radiation pattern stability using a signal processing approach would require a tradeoff between pattern control and maximum attainable sensitivity.

Directions for future work include the study of larger arrays, broadband systems, and the effects of mutual coupling on sensitivity and noise performance. Further study of practical signal processing algorithms is required, as well as the possibility of using an auxiliary antenna in conjunction with the array feed. Finally, remaining technical hurdles connected with practical realization of an array feed system with astronomically useful sensitivity should be addressed and a prototype array feed constructed and tested with signal processing for RFI mitigation on an existing radio astronomy platform.

Acknowledgments.

This work was supported by the National Science Foundation grant number AST-9987339.

References

Amitay, N., and H. Zucker (1972), Compensation of spherical reflector aberrations by planar array feeds, *IEEE Trans. Ant. Propag.*, *20*(1), 49–56.

Baan, W. A., P. A. Fridman, and R. P. Millenaar (2002), RFI mitigation at WSRT: algorithms, test observations, system implementation, in *Proceedings of the URSI General Assembly XXVII.*

Barnbaum, C., and R. F. Bradley (1998), A new approach to interference excision in radio astronomy: Real-time adaptive cancellation, *Astronomical Journal*, *116*, 2598–2614.

Bell, J. F., P. J. Hall, R. J. Sault, and L. Kewley (2000), Implementing Interference Suppression: Impacts on SKA System Design, in *Technological Pathways to the SKA*, Jodrell Bank, Manchester, http://www.jb.man.ac.uk/ska/workshop/Bell2.pdf.

Bij de Vaate, J. G., and G. W. Kant (2002), The phased array approach to SKA, results of a demonstrator project, in *Proceedings of the European Microwave Conference*, Milan.

Bird, T. S. (1982), Contoured-beam synthesis for array-fed reflector antennas by field correlation, *IEE Proc. H*, *129*, 293–298.

Bird, T. S., J. L. Boomars, and P. J. B. Clarricoats (1978), Multiple-beam dual-offset reflector antenna with an array feed, *Electron. Lett.*, *14*, 439–441.

Blank, S. J., and W. A. Imbriale (1988), Array feed synthesis for correction of reflector distortion and vernier beamsteering, in *IEEE Transactions on Antennas and Propagation*, vol. AP-36, pp. 1351–1358.

Bower, G. C. (2002), A radio frequency interference mitigation strategy for the Allen telescope array, in *Proceedings of the URSI General Assembly XXVII.*

Bradley, R. F., K. Saini, and J. R. Fisher (1996), A prototype array feed - design and construction, in *Proceedings of USNC/URSI Meeting*, Boulder, Colorado.

Briggs, F., J. Bell, and J. Kesteven (2000), Removing radio interference from contaminated astronomical spectra using an independent reference signal and closure relations, *Astronomical Journal*, *120*, 3351–3361.

Ellingson, S. (2003), Beamforming and interference canceling with very large wideband arrays, *IEEE Trans. Antennas Propagat.*, *51*(6), 1338–1346.

Ellingson, S., and G. Hampson (2002), A subspace-tracking approach to interference nulling for phased array-based radio telescopes, *IEEE Trans. Antennas Propagat.*, *50*(1), 25–30.

Ellingson, S. W., J. D. Bunton, and J. F. Bell (2001), Removal of the GLONASS C/A Signal from OH Spectral Line Observations using a Parametric Modelling Technique, in *The Astrophysical Journal Supplement Series*, 135, pp. 87–93.

Emerson, D., and J. Payne (Eds.) (1995), *Astronomical Society of the Pacific Conference Series, Multi-Feed Systems for Radio Telescopes.*, vol. 75, Astronomical Society of the Pacific, San Francisco.

Fisher, J. R. (1996), Phased array feeds for low noise reflector antennas, NRAO Electronics Division Internal Report 307, http://www.gb.nrao.edu/ rfisher/Papers/af_ieee.ps.

Fisher, J. R. (1999), Techniques for coping with RFI, in *Preserving the Astronomical Sky*, IAU Symposium 196, Vienna, http://www.gb.nrao.edu/ rfisher/Papers/iau196.ps.

Fisher, J. R. (2001), RFI and how to deal with it, in *NRAO Papers*, www.gb.nrao.edu/ rfisher/Papers/rfi_sumschool.ps.

Fisher, J. R., and R. F. Bradley (1998), Technical progress on array feeds and RFI cancellation, in *International Square-Kilometer Array Science Meeting*, Calgary, Canada.

Fisher, J. R., and R. F. Bradley (1999), Full-Sampling Focal Plane Array, in *Proceedings of Imaging at Radio through Submillimeter Wavelengths Workshop, ASP Conference Series No. 217*, edited by J. Mangum and S. J .E. Radford, pp. 11–18, Tucson, AZ.

Fisher, J. R., and R. F. Bradley (2000), Full sampling array feeds for radio telescopes, in *Proceedings of the SPIE International Symposium on Astronomical Telescopes and Instrumentation*, vol. 4015, pp. 308–319.

Fisher, J. R., R. F. Bradley, R. Escoffer, and K. Saini (1996), Phased array feed design and prototype, in *Proceedings of the URSI General Assembly*, Lille, France.

Fridman, P., and W. Baan (2001), RFI mitigation methods in radio astronomy, *Astronomy & Astrophysics*, *378*, 327–344.

Galindo-Isreal, V., S. Lee, and R. Mittra (1978), Synthesis of a laterally displaced cluster feed for a reflector antenna with application to multiple beams and contoured patterns, *IEEE Trans. Ant. Propag.*, *26*(2), 220–228.

Hall, W. J., P. C. Wilcockson, M. H. Skeen, S. J. Stirland, L. Hilliard, H. S. Ghuman, and L. E. Comtesse (1989), Satellite antenna subsystem using shaped reflector and multiple feed gridded reflectors, in *IEEE Antennas and Propagation Society International Symposium Digest*, vol. 1, pp. 60–64.

Hsiao, F.-R., and K.-L. Wong (2004), Omnidirectional planar folded dipole antenna, *IEEE Trans. Ant. Propag.*, *52*(7), 1898–1902.

Huang, J., and V. Jamnejad (1989), A microstrip array feed for land mobile satellite reflector antennas, *IEEE Transactions on Antennas and Propagation*, *37*, 153–158.

Imbriale, W. A., P. G. Ingerson, and W. C. Wong (1974), Large lateral feed displacements in a parabolic reflector, *IEEE Trans. Ant. Propag.*, *AP-22*(6), 742–745.

Ivashina, M., and C. van't Klooster (2002), Focal fields in reflector antennas and associated array feed synthesis for high efficiency multi-beam performances, in *Proceedings of the ESTEC Antenna Workshop*, Noordwijk, The Netherlands.

Jeffs, B. D., L. Li, and K. F. Warnick (2004), Auxiliary assisted interference mitigation for radio astronomy arrays, *IEEE Trans. Signal Process.*, in press.

Karimi, J., and S. Blostein (1996), Parabolic reflector array signal processing for improved rural area coverage in personal satellite communications, in *1996 5th IEEE International Conference on Universal Personal Communications*, vol. 1.

Lam, P. T., S. Lee, D. C. Chang, and K. C. Lang (1985), Directivity Optimization of a Reflector Antenna with Cluster Feeds: A Closed-Form Solution, *IEEE Transactions on Antennas and Propagation*, *AP-33*(11), 1163–1174.

Mailloux, R. J. (1994), *Phased Array Antenna Handbook*, Artech House.

Mrstik, A., and P. Smith (1981), Scanning capabilities of large parabolic cylinder reflector antennas with phased-array feeds, in *IEEE Transactions on Antennas and Propagation*, vol. 29, pp. 455–462.

Perrott, R. A., and J. M. Griffin (1991), L-band antenna systems design, in *IEEE Colloquium on INMARSAT-3*.

Poulsen, A. J., B. Jeffs, K. Warnick, and R. Fisher (2003), Real-time Adaptive Cancellation of GLONASS Interference in OH Signal Observations at the Green Bank Telescope, in *Proceedings of the IEEE APS-URSI Symposium*, Columbus, Ohio.

Raza, J., A.-J. Boonstra, and A.-J. van der Veen (2002), Spatial filtering of RF interference in radio astronomy, *IEEE Signal Processing Lett.*, *9*(2), 64–67.

Reid, M. S., and D. A. Bathker (1972), Low Noise Microwave Receiving Systems on a 64 m Antenna, in *Microwave Symposium Digest, GMTT International*, vol. 72, pp. 17–20.

Rudge, A. W., and M. J. Withers (1971), New techniques for beam steering with fixed parabolic reflector, *Proc. IEE*, *118*, 857–863.

Shelton, P. (1965), Multiple-feed systems for objectives, in *IEEE Transactions on Antennas and Propagation*, vol. 13, pp. 992–994.

Shin, J., and D. H. Schaubert (1999), A parameter study of stripline-fed Vivaldi notch-antenna arrays, *IEEE Trans. Ant. Propag.*, *47*(5), 879–886.

Singh, A. K., and G. Kumar (1996), EMCP microstrip antennas as feed for satellite receiver, in *IEEE Antennas and Propagation Society International Symposium Digest*, vol. 2, pp. 1274–1277.

Smolders, B., and G. Hampson (2002), Deterministic RF nulling in phased arrays for the next generation of radio telescopes, *IEEE Antennas Propagat. Mag.*, *44*(4), 13–22.

Stavely-Smith, L., et al. (1996), The Parkes 21 cm multibeam receiver, *Publ. Astron. Soc. Aust.*, *13*(3), 243–248.

Uzsoky, M., and L. Solymar (1956), Theory of superdirective linear arrays, *Acta Phys. Acad. Sci. Hung.*, *6*, 195.

Weber, R., B. Lamarque, and R. Canals (1999), Two Examples of Real-time RFI Detectors for Time-blanking, in *Proceedings of the URSI 26th General Assembly*, Toronto.

Woo, K. (1986), Multiple beam antenna feed development, in *IEEE Antennas and Propagation Society International Symposium Digest*, pp. 409–412.

(Received _____.)